STUDIUL MECANISMULUI DE REACȚIE ÎN BETONUL CELULAR AUTOCLAVIZAT CU CONȚINUT DE DEȘEURI DE MINEREU CU FIER
STUDY ON THE REACTION MECHANISM OF AUTOCLAVED AERATED CONCRETE BASED ON IRON ORE TAILINGS

XIAO-WEI CUI[1, 2], CHANG-LONG WANG[3,4] *, WEN NI[1, *], YAN-QING DI[2], HAN-LONG CUI[3], LIE CHEN[3],

[1] *Beijing Key Laboratory on Resource-oriented Treatment of Industrial Pollutant, University of Science and Technology Beijing, Beijing 100083, China.*
[2] *Shaanxi Key Laboratory of Comprehensive Utilization of Tailings Resources, Shangluo University, Shangluo Shaanxi Province 726000, China.*
[3] *Jiangxi Key Laboratory of Mining & Metallurgy Environmental Pollution Control, Jiangxi University of Science and Technology, Ganzhou Jiangxi Province 341000, China*
[4] *School of Civil Engineering, Hebei University of Engineering, Handan Hebei Province, 056038, China*

To comprehensively utilize iron ore tailings (IOT), it was used as main siliceous materials in autoclaved aerated concrete (ACC) with excellent mechanical properties in this study. The physical and mechanical properties of AAC were analyzed by using X-ray diffraction analysis (XRD), fourier transform-infrared spectroscopy (FT-IR), thermogravimetric/differential scanning calorimeter (TG-DSC) and scanning electron microscope (SEM). The hydration products and microstructure with different stages of AAC were detected. The results show that that the main hydration products including ettringite (AFt), low crystallinity of C-S-H gels and $Ca(OH)_2$ were generated before the autoclaving. After the autoclaving, the major hydration products were tobermorite, C-S-H gels and hibschite in the final AAC, AFt was decomposed. XRD diffraction peaks of the original mineral composition in IOT were reduced, which indicated that the mineral composition of IOT were decomposed, and the reaction between active components of SiO_2, Al_2O_3 and $Ca(OH)_2$ caused the formation of tobermorite under conditions of high temperature and pressure and hot alkaline activation.

1. Introduction

Autoclaved aerated concrete (AAC) is a kind of green building material with a unique cellular structure that provides high thermal efficiency, superior fire resistance and excellent acoustical absorbing abilities [1,2]. It can be used as a substitution for fired clay brick with the benefits for farmland conservation, environmental protection, and energy saving [3]. The basic ingredients of AAC are calcareous materials (cement and lime) and siliceous materials (sand or fly ash), and an expansion agent—aluminum powder. In some areas, the shortage of high silica content sand limited the production and application of AAC. However, there is a large amount of silica in metal ore mining. That is the reason why iron ore tailing (IOT) was chosen for the present work.

Iron ore tailings (IOT) in China have been nearly totally piled up through the history of iron production. Now more than 50 billion metric tons of iron ore tailings are estimated to exist in China, posing a severe threat to the environmental condition [4]. IOT is most difficultly reused in the traditional building materials, due to its nature very fine grain size. It has been reported that IOT can be used to prepare building materials such as high-strength concrete [5-8], cementitious materials or cement [9-14], autoclaved lime-sand brick [15,16] and so on. The fine IOT particles obtained by crushing, grinding and milling contains large amounts of silicate minerals, which is of big difference in aspects of physical and chemical properties compared with conventional acidic material used to produce AAC material. The active ingredients of silicate minerals such as Al_2O_3 and SiO_2 are prone to carry on hydration reaction at high temperature and high pressure alkaline hydrothermal environment and produce hydrate calcium silicate hydrates. To extend the range of raw materials and lower the production costs, several researchers have investigated the possibility of replacing the traditional raw materials of AAC by industrial waste, such as coal bottom ash [2], phosphorus slag and efflorescence sand [17], air-cooled slag [18], copper tailings [4] and. lead–zinc tailings [19]. Using quartz—bearing tailings as a supplement for natural and/or artificial sand to produce AAC is a promising way to solve both the resource problem of sand shortage and the environmental problems caused by the tailings.

In this study, IOT was used as main raw

---

* Autor corespondent/*Corresponding author*,
E-mail: 13716996653@139.com, niwen@ces.ustb.edu.cn.

materials to prepare AAC. The physical and mechanical properties of AAC were analyzed by using XRD, FT-IR, TG-DSC and SEM. The hydration products and microstructure within AAC will be analyzed as well.

2. Materials and Methods

2.1. Experimental materials

The AAC samples were prepared using the following raw materials: IOT, Silica sand (SS), Fly ash (FA) lime (L), 42.5 Portland cement (OPC) and the gypsum of flue gas desulfurization waste (FGDW). The chemical compositions of the raw materials are listed in Table 1.

IOT. Typical IOT samples are first taken randomly many times from several production lines in the ore-dressing workshops of the Haoyang Mining Co., Ltd. at Lingqiu county, Shanxi province, undergoing precipitation, stoving, blending and splitting. Table 1 shows that the amount of SiO_2 in the IOT was approximately 54.41 %, and the level of residual iron in the tailing, which was present in the form of magnetite, was approximately 14.54 %. The IOT thus were of a low-silicon high-iron magnetite-quartzite type. The 0.08 mm sieve residual of IOT was 68.32%.

SS. The research uses wind-blown sand in industrial production from the Beijing BBMG AAC Co. Ltd. Its chemical composition is in Table 1, from which it is seen that the SiO_2 content of SS satisfies operational requirements.

FA. The research uses FA in industrial production from Hebei Datang International Tangshan Thermal Power Co., Ltd. Its chemical composition is in Table 1. Table 1 shows that the amount of SiO_2 in the IOT was approximately 77.52 %. The silicon content of FA conforms to the requirement of preparing AAC for raw materials.

OPC. The initial and final setting times of OPC were 110 min and 210 min, respectively.

L. The composition of L is shown in Table 1and the content of effective CaO was 71%. The digestion time of L was 15 min, and the digestion temperature was 65 ºC. The 0.08 mm square hole sieve residual of L was less than 12 %.

FGDW. The primary mineral phase of FGDW is $CaSO_4·2H_2O$. The specific surface area of the FGDW is 389 m^2 kg^{-1}. Its chemical compositions are listed in Table 1, and 0.08 mm sieve residual is less than 7.9%.

Other materials. Aluminum powder paste in oil was used as the foaming agent using and the foam stabilizer is a specific mixture of oleic acid, triethanolamine and water at room temperature.

2.2. Experimental Method
2.2.1. Preparation of AAC

Firstly, IOT, SS and FA were respectively dried in oven at 105 ºC for 24 h to make moisture content less than 1 %. Then, crushed using SM φ 500 mm × 500 mm laboratory ball mill to yield a specific surface area of abouy 350 m^2 kg^{-1}. The prepared powder of the raw materials were thoroughly dry mixed. Then warm water (55 ± 1 ºC) was added and mixed for 90 s. Finally, Then aluminium powder was added into the slurries with additional 40 s stirring. Poured the slurry into the triple-mold molds (100mm×100mm×100mm), then cured at 60 ºC for 4 h under a steam saturated condition. After their swollen up surface being cut to flat, the samples were demolded and put into an industrial autoclave for hydrothermal reaction for 8 h (the highest pressure is 1.25 MPa, and the highest temperature 185 ºC).

2.2.2. Sample characterisation

The bulk density and compressive strength of the AAC samples were tested according to GB/T 11968-2008 norm [20]. For bulk density measurements, three samples of each AAC mixture were oven dried at 60 ± 5 ºC for 24 hrs, then at 80 ± 5 ºC for 24 hrs, and finally at 105 ± 5 ºC for 24 hrs, consecutively. The mass of the oven dried samples were used to calculate the bulk density. The compressive strength were performed on three samples of each AAC mixture with a moisture content of 8-12 % at a loading rate of 2.0 ± 0.5 kN/s.

The X-ray diffraction (XRD) spectra of the AAC samples were performed using a D/Max-RC diffractometer (Japan) with CuKα radiation, voltage of 40 kV, current of 150 mA and 2θ scanning ranging between 5 º and 90 º. The functional groups vibration of each sample was qualitatively analyzed by NEXUS70 Fourier transform infrared (FT-IR, test range 350~4000 cm^{-1}). The DSC-TG analysis of the AAC samples was performed from 20 to 1000 ºC at a rate of 10 ºC/min using a Netzsch STA 449C thermal analyser with dry air as the stripping gas. FESEM observation was performed to analyse the hydration products of the

Table 1

Chemical composition of raw materials (mass fraction, %)

Materials	SiO_2	Al_2O_3	Fe_2O_3	FeO	CaO	MgO	Na_2O	K_2O	SO_3	MnO	Loss
IOT	54.41	7.99	8.94	10.65	5.06	5.75	0.98	0.43	1.26	0.03	2.9
SS	87.07	5.87	0.64	0.19	1.34	0.97	1	1.9	—	0.02	0.93
L	7.31	3.32	3.21	0.48	75.64	2.96	—	1.63	0.53	0.04	4.18
C	26.12	5.75	3.17	0.93	57.29	1.53	0.54	0.31	—	0.12	4.02
FGDW	2.64	0.84	0.08	0.22	43.65	0.14	0.21	0.23	31.16	—	—

Table 2

Material proportions, physical and mechanical properties of AAC sample

Mixture composition of AAC (wt%)					Dry density (kg m^{-3})	Compressive strength (MPa)	DCS (MPa)	Specific strength
IOT	SS	OPC	L	FGDW				
42	20	9	24	5	592	3.82	4.94	8.34

1-Quartz   2-Plagicoclase   3-Chlorite   4-Biotite   5-Hornblende   6-Grunerite
7-Augite   8-Magnetite   9-Pyrite   a-Hibschite   b-Calcite   c-Ferrotschermakite
d-Anhydrite   e-Tobermorite   f-Portlandite   g-Ettringite   h-Anorthite   i-Albite
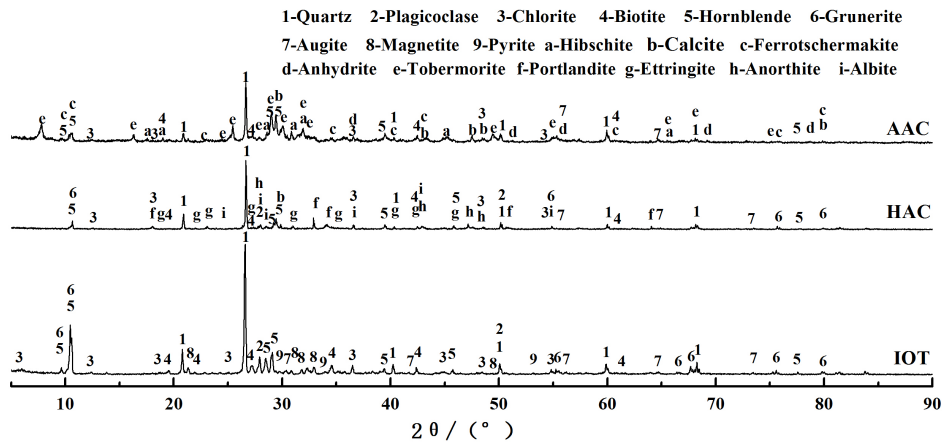
Fig. 1 – XRD pattern of IOT, HAC and AAC samples.

AAC samples using a Zeiss SUPRA™55 scanning electron microscope coupled with a Be4-U92 energy spectrum. The AAC samples should be carbon sprayed before FESEM testing.

3. Results and Discussion

3.1. Physical and mechanical properties

The results of test of the AAC samples prepared IOT, SS and FA and its related raw materials proportions are given in Table 2. IOT content was 42% of the total solid mixture and aluminum powder content was 0.056%. The water/solid ratio was 0.56. At the designed proportions, the compressive strength of AAC samples could get 3.82 MPa and the dry density of AAC was 592 kg m^{-3}, which passed the requirements of A3.5, B06 level of AAC sample regulated by GB/T 11969-2008 [20]. Additionally, the compressive strength of sample in the absolute dry condition (DCS) can reach up to 4.94 MPa, and its corresponding specific strength reaches as high as 8.34.The indices of AAC prepared with IOT as the main raw material can be achieved requirements with SS and FA. The results suggested that IOT of low-silicon high-iron magnetite-quartzite type can be used as silica materials in the AAC production, which may solve the problems of AAC production in some regions of China, where SS and FA shows apparent shortage.

3.2. XRD analyses

Figure1 showed the XRD pattern of AAC sample, its related hardened aerated concrete (HAC) sample precured under the saturated steam curing for 4 h after being mixed with warm water and original IOT. The curve of original IOT in Figure 1 identified that most of the minerals were well crystallized, which suggested by the sharp diffraction peaks and low back ground. The main minerals are quartz (SiO_2), hornblende ($Al_{3.2}Ca_{3.4}Fe_{4.02}K_{0.6}Mg_6NaSi_{12.8}O_{44}(OH)_4$), grunerite ($Fe_7Si_8O_{22}(OH)_2$) and plagioclase ($NaAlSi_3O_8$), accompanied by minor phases including chlorite ($(Mg,Fe)_{4.75}Al_{1.25+}(Al_{1.25}Si_{2.75}O_{10})$ $(OH)_8$), biotite ($K(Mg,Fe)_3AlSi_3O_{10}(F,OH)_2$), augite ($(Ca,Mg,Fe,Al)_2(Si,Al)_2O_6$), magnetite ($Fe_3O_4$) and pyrite ($FeS_2$).

In HAC's spectrum in Figure 1, it was shown that apart from the minerals of IOT, after being precured around 60 °C for 4 h. Compared with the original IOT, newly formed ettringite ($3CaO·Al_2O_3·3CaSO_4·32H_2O$), portlandite ($Ca(OH)_2$), anorthite ($Ca(Al_2Si_2O_8)$) and albite could be observed, and the main XRD diffraction peaks of mineral composition of the original IOT decreased. Among them, $Ca(OH)_2$ formed due to lime hydration and OPC hydration while the formation of AFt mainly came from two parts. One was that the ultrafine particles in IOT and SS partly reacts with $Ca(OH)_2$ to form hydrated calcium silicate (C-S-H gels) and hydrated calcium aluminate crystals. The other was that hydration

calcium aluminate (C-A-H) reacted with SO_4^{2-}ions of FGDW to form AFt crystal rapidly forms from the reaction of hydrated calcium aluminate with FGDW in the early hydration period. At the same time, the broad band at around of "convex closure" in two theta range between 26–34 ° indicated that there is amorphous diffraction (no) of amorphous and low crystallized C-S-H gels [21]. Comparing spectra of IOT and HAC, the characteristic peaks of quartz and plagicoclase decreased significantly. That means these crystalline minerals in IOT, which were inert after being precured around 60 ºC for 4 h, participated in the hydration reaction forming AFt, C-S-H gel during the procuring process. As indicated in HAC's spectrum, most minerals of magnetite and pyrite in IOT are not detected. The non-detection of magnetite and pyrite is likely due to the fact that the overall amount of those minerals originally comprising small amount in IOT are in more minor quantities after addition into the dry mixture with only 42% in weight, so that the XRD is not sensitive enough to allow detection at such low level [4].

From spectrum of AAC, it can be seen that the major minerals in the final AAC products are tobermorite-11 Å ($Ca_5(OH)_2Si_6O_{16}\cdot4H_2O$), hibschite ($Al_2O_3(CaO)_3(H_2O)6$), anhydrite($CaSO_4$), hornblende, ferrotschermakite ($Ca_2Fe_3Al_2(Si_6Al_2)O_{22}(OH)_2$)and residual minerals quartz, accompanied by calcite ($CaCO_3$), chlorite, biotite and augite in minor quantities. Plagicoclase, anorthite and albite ($NaAlSi_3O_8$)from IOT and SS were not detected. That is to say the minerals in IOT and SS were evidently involved into the hydrothermal reaction during the 8 h autoclaving process.

In the AAC sample autoclaved beginning stages, the insufficient amount of dissolved Si^{4+} ions and Al^{3+} ions from IOT and SS were present with an excessive amount of $Ca(OH)_2$, resulting in the formation of a small amount of tobermorite-11 Å [22]. As the autoclaving time extended, a large amount of Si^{4+} ions and Al^{3+} ions were dissoveld from both IOT and SS in alkaline hydrothermal conditions, which promoted the formation of tobermorite. Meanwhile, the disappeared intensity of the plagicoclase, anorthite and albite peaks indicated that more tobermorite formed and $Ca(OH)_2$ was depleted during the autoclaving since the diffraction peaks of tobermorite displayed an increasing trend and the peaks of $Ca(OH)_2$ disappeared. Before the autoclaving, AFt formed by the reaction of calcium aluminate hydrate (C-A-H) from OPC with SO_4^{2-} ions of FGDW. Then, AFt was decomposed into monosulfoaluminate hydrate (AFm), SO_4^{2-} ions and Al^{3+} ions at a temperature of approximately 70 ºC [23]. During the autoclaving, AFm was continuouely decomposed into $CaSO_4$ and tricalcium aluminate hexahydrate (C_3AH_6). Thus, after the autoclaving, the diffraction peaks of anhydrite in AAC products were.

Hibschite belongs to the hydrogarnet class. Because of the presence of Al in IOT, the hydrogarnet phase first precipitated from the CaO-Al_2O_3-SiO_2-H_2O system. However, Continuous autoclaving would help reduce the amount of OH^- ions and thus promote another aluminium silicate phase, e.g., tobermorite [22,24], which would influence the AAC properties [25]. Hibschite was able to precipitate rapidly in a wide temperature range due to massive calcium interaction with the dissolved Si^{4+} ions and Al^{3+} ions from both IOTS and SS during the autoclaving [26]. Because of the limited time of autoclaving, the hydrate hessonite garnet would undergo an incomplete transformation to tobermorite, and thus both were present in the AAC products.

The ferrotschermakite phase in the AAC products was a double chain structure, the reason was due to the grunerite in IOT occured ion exchange between Al^{3+}, Si^{4+}, Ca^{2+} and Fe^{2+} through autoclaving process. Calcite ($CaCO_3$) also occurred in the AAC products, which is a frequently encountered phase in most of the calcium-rich building materials formed by absorbing CO_2 in the atmosphere [27].

The calcite, ferrotschermakite, anhydrite together with non-reacted hornblende, biotite, chlorite augite and residual minerals quartz would become the primary aggregate in the AAC samples.

3.3. FT-IR analysis

Figure 2 shows FT-IR patterns of HAC and AAC samples. As shown, the absorption peaks move towards lower wave-numbers. It can be seen from HAC's spectrum, after being precured around 60 ºC for 4 h, the strongest absorption region 1250~1100 cm^{-1}, the weak band 1160~1250 cm^{-1} and the strong band 1076~1100 cm^{-1}, belonged to the absorption band of quartz and related to anti-symmetric stretching mode of Si-O, respectively. The absorption banded at 1080, 779 and 462 cm^{-1} can be attributed to anti-symmetric stretching mode of Si-O, symmetric stretching mode of Si-O-Si, bending mode of Si-O, respectively.
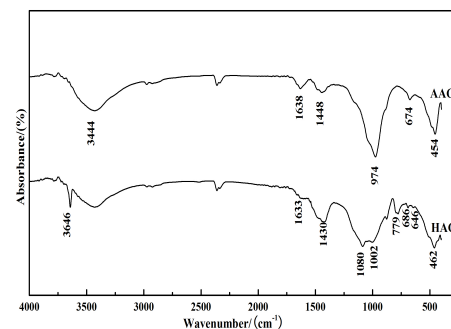

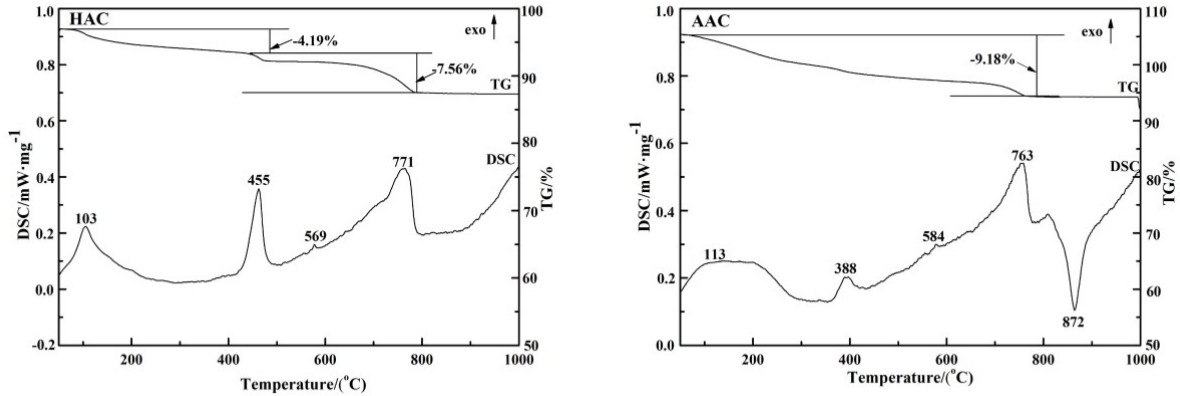
Fig. 2 – FT – IR patterns of HAC and AAC samples.

Fig. 3 – TG – DSC patterns of HAC and AAC samples.

Wavenumber around 3646 cm^{-1} absorption band was the result of Ca (OH)$_2$ stretching vibration of the hydroxyl group. Wavenumber characteristic peak at 3444cm^{-1} came from stretching vibration of the adsorbed water in C-S-H gels and AFt. Bending vibration wave number at about 1633 cm^{-1} absorption band was attributed to hydroxyl in the absorbed water in C-S-H gels and AFt. Asymmetric stretching vibration absorption banded in the wave number at 1430 cm^{-1} belonged to CO$_3^{2-}$ in calcite due to carbonization. Wavenumber in the broader band 1000 cm^{-1} ~ 1050 cm^{-1} can be attributed to the stretching vibration around Si-O bond in C-S-H gels. Wavenumber in 640 ~ 700 cm^{-1} was characterized as O-Si (Al) -O bending vibration, which belonged to the vibration bands of plagicoclase in IOT.

In Figure 2, curve 2 belongs to AAC sample. However, the characteristic bands of quartz group minerals at 1080, 1002, 779, 686, 646 and 462 cm^{-1} disappear, which suggested that the amount of formed hydration products increased after autoclaved and they tended to crystalize. The decomposition of AFt at high temperatures was confirmed by the disappearance of absorption band at 1638 cm^{-1} belonging to AFt. Meanwhile new characteristic peaks at 1633 cm^{-1}, 974 cm^{-1} and 451cm^{-1} observed in AAC were related to the bending mode in H$_2$O, the symmetric stretching mode of Si-O in [SiO$_4$] structure Q^2, and the bending mode of Si-O, respectively. The strong infrared active of stretching vibration of Si-O led to high intensity band at 974 cm^{-1}, which was attributed to the layered structure of tobermorite, then 454 cm^{-1} belonged to hibschite.

3.4. TG-DSC analysis

Figure 3 are TG-DSC profiles of HAC and AAC samples before and after autoclaved , respectively. As shown in Figure 3, a broad endothermic peak exists in the range of 80~200 ºC, which can be attributed to the dehydration of AFt and C-S-H gels [28].

There were varying endothermic peaks at

103ºC, 455 ºC, 569 ºC and 771 ºC, as indicated in HAC. There was mass loss of 4.19% belonging to the relatively sharp endothermic peak at 103 ºC, which results from the dehydration of calcium silicate hydrates with low crystallinity degree and AFt. The endothermic peak at 455 ºC was the outcome of the decomposition of Ca(OH)$_2$. The endothermic peak at 569 ºC mainly suggested the transition of β-quartz to α-quartz [29] in IOT while no mass loss was obtained in TG profile. The endothermic peak at 771 ºC was supposed to be caused by the dihydroxylation of C-S-H gels as well as the decomposition of calcite.

In AAC, one can observe a wide and flat endothermic peak at 50 ºC~350 ºC due to zhe removal of free water, absorbed water or weak crystal water of some hydration products. The endothermic peak at 388 ºC was the dehydration of the hydration products of tobermorite, C-S-H gels and hibschite. The TG-DSC research by Klimesch et al. [30] showed that C-S-H can transit to okenite via dihydroxylation at 840 ºC~900 ºC and the transition temperature increased as the amount of Al^{3+} in C-S-H increases. Thus, the exothermic peak at 872 ºC was the result of the transition of tobermorite, which was the main reaction hydration products in AAC samples. And it should be noticed that there was no endothermic peak belonging to the dehydration of Ca(OH)$_2$ and this indicated its entire consumption via reaction during autoclaving, which was in good accordance with the XRD results in Section 3.2 and FTIR results in Section 3.3.

3.5. FE-SEM analysis

Figure 4 illustrated FE-SEM and EDS of HAC. The surface microstructure of wall section in HAC sample (Fig. 4 (a1), (a2)) showed that, the main hydration products in HAC sample before static maintenance include poor crystallized C-S-H gels and needle-shaped AFt, there were no other crystalline hydration products formed, and the observation was in accordance with the XRD analysis in Section 3.2. The ED spectroscopy of
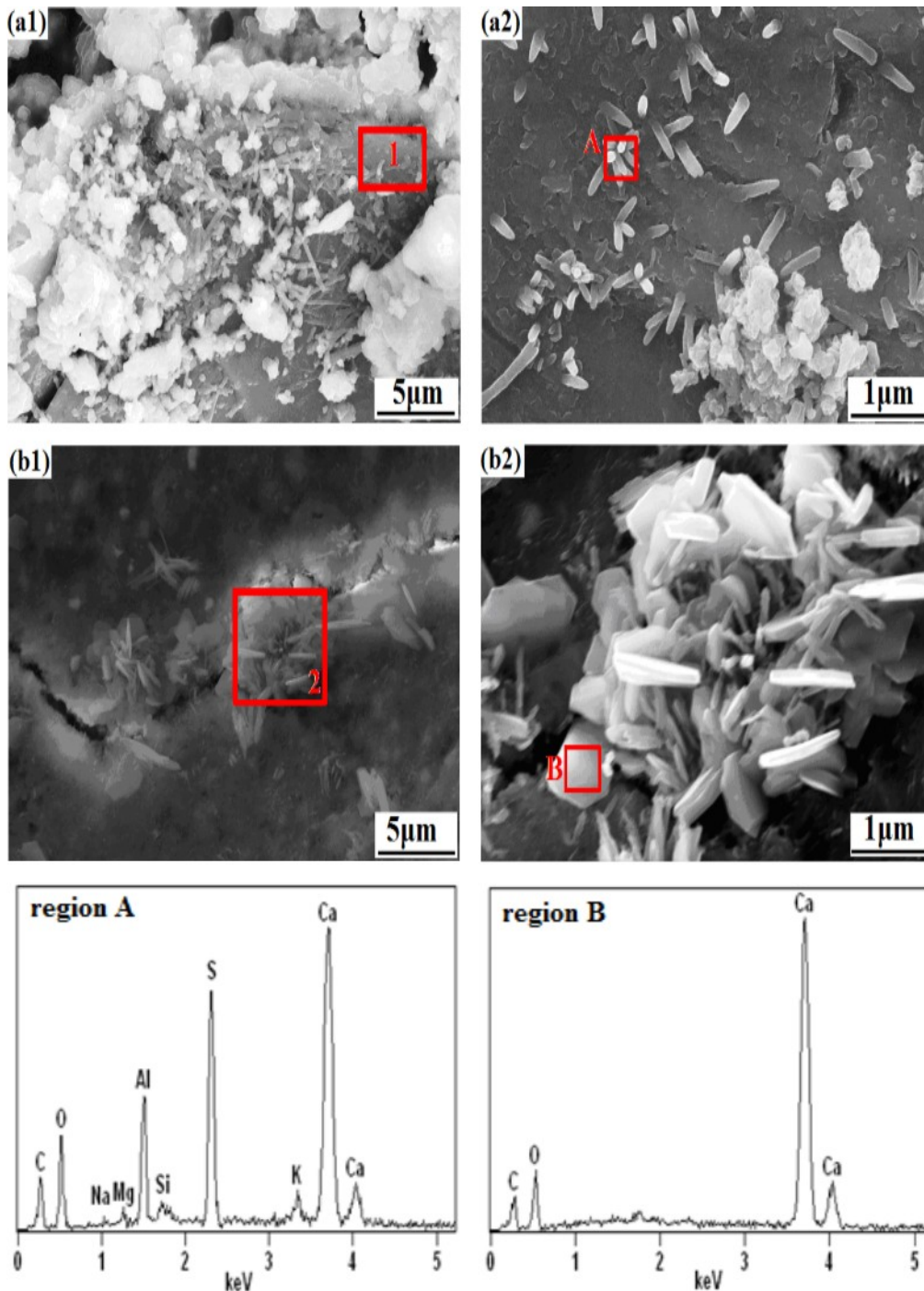
Fig. 4 – FESEM and EDS of HAC sample (a1 surface of wall section; b1 – inner surface of one artificial pore; a2, b2 further magnification of a1, b1).

marked region 1 in Figure 4 (a1) showed that the main elements in that area were Ca, S and Al, which were the same as AFt. C-S-H gels mainly formed due to the hydration of cement in AAC while AFt forms due to the reaction of gypsum and calcium aluminate hydrates. The inner surface of one artificial pore in HAC sample (Fig. 4 (b1), (b2)) showed that, except for Ca(OH)$_2$, there was no other crystalline hydration products formed, the hydration products Ca(OH)$_2$ showed in slab-flaky in Figure 4 (b2), the spectroscopy of marked region 2 showed that the main element in that area was Ca, which were the same as Ca(OH)$_2$.

Figure 5 showed the microstructure of AAC sample after autoclaved for 12 h. which were mainly tobermorite and C-S-H. A large amount of plate-shaped tobermorite with the thickness of about 0.1 ~ 0.2 μm can be observed in Figure 5 (a2). The crystallinity of plate-shaped tobermorite occured after autoclaved, and they intertwine together to forming the skeleton structure of AAC products, which contributes to the strength of AAC in Fig.5 (b1) and (b2). The EDS spectrum of region 1 in Fig. 5(b2) showed that Al exists in the plate-shaped hydrates due to the partial substitution of [SiO$_4$] by [AlO$_4$] [31]. Hydration products in the
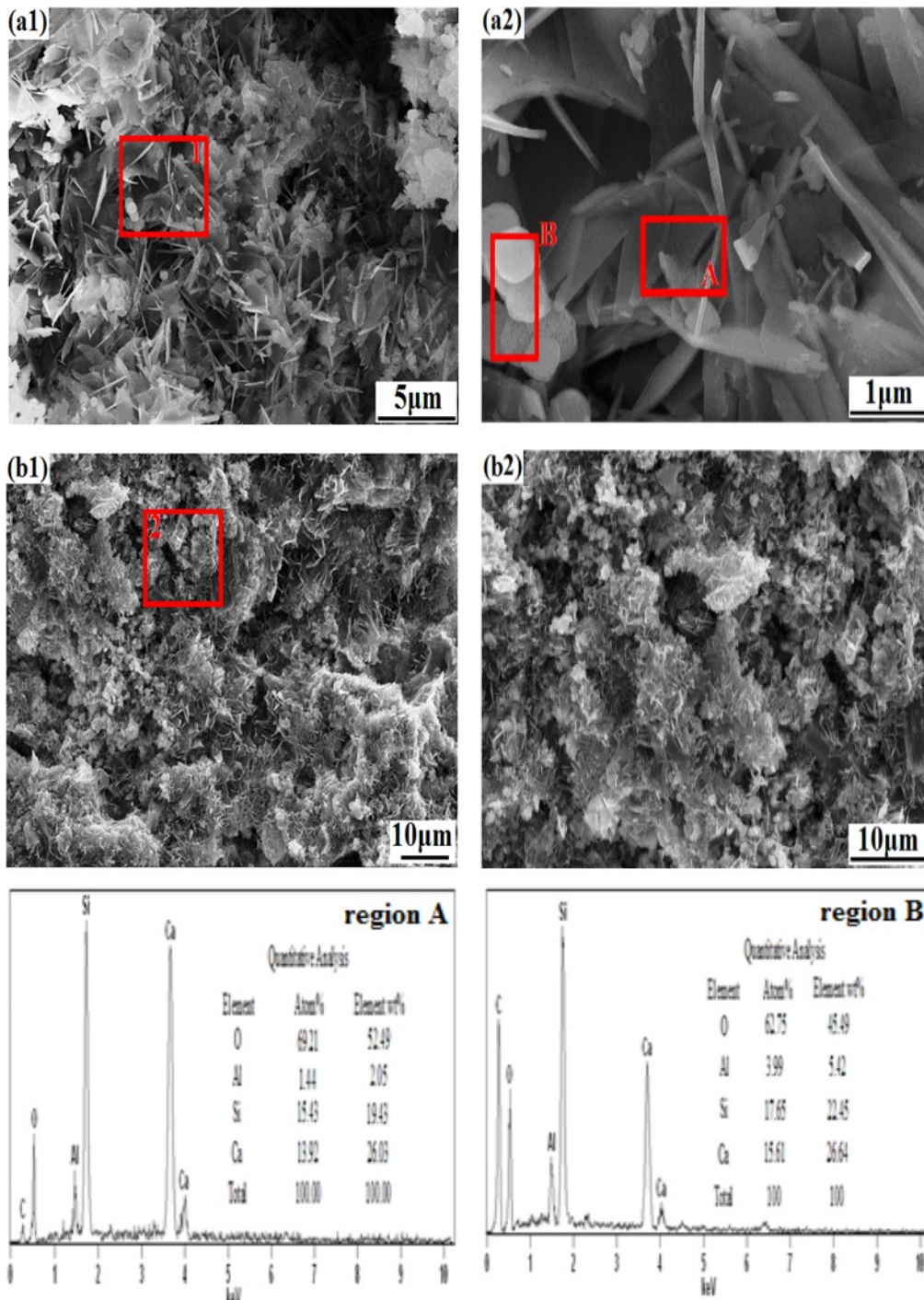
Fig. 5 – FESEM and EDS of AAC sample (a1 surface of wall section; b1 – inner surface of one artificial pore; a2, b2 further magnification of a1, b1).

region 2 $nCa/n(Si+Al) = 0.8326$ can be obtained, which was the same as that of tobermorite ($Ca_5(OH)_2Si_6O_{16}\cdot4H_2O$) $n(Ca)/n(Si) = 0.8333$. After autoclaved, the solubility of active SiO_2 and Al_2O_3 in IOT—increased in alkaline water heat environment and ability to participate in chemical reactions enhanced, which played a positive role in improving the crystallinity of hydration products. There was hibschite with globular or botryoidalis morphology in the range of 0.5-1 μm (at point B in Fig. 5 (a2)) in the AAC samples. The compostion of phase contained a ratio of nCa/n(Si+Al)=0.721, which was equal to that of hibschite (0.721).

4. Conclusions

In this study, the material compositions, physical and mechanical properties and hydration products of AAC were investigated. Based on these analyses, the following conclusions may be drawn:

(1) IOT could be used to prepared AAC as the main siliceous raw materials in substitution of fly-ash and quartz sand. This may develop a way to utilize the iron ore tailings for reuse.

(2)The sample with a compressive strength of 3.82 MPa and a bulk density of 592 kg·m^{-3} could

be obtained by an optimized raw materials composition of iron ore tailings of 42%, silica sand of 20%, cement of 9%, lime of 24% and gypsum of 5% in laboratory.

(3) Before the autoclaving, the hydration products in assessed in HAC were AFt, $Ca(OH)_2$ and C-S-H gels. During the autoclaving, AFt was decomposed and more tobermorite was formed as well as C-S-H gels and hibschite.

REFERENCES

1. N. Narayanan and K. Ramamurthy, Structure and properties of aerated concrete: a review, Cement and Concrete Research, 2000, **22**(5), 321.
2. H. Kurama, I.B. Topçu and C. Karakurt, Properties of the autoclaved aerated concrete produced from coal bottom ash, Journal of Materials Processing Technology, 2009, **209**(2), 767.
3. T. Piyush, Energy efficiency and building construction in India, Building and Environment, 2001, **36**(10),1127.
4. X.Y. Huang, W. Ni, W.H. Cui, Z.J. Wang and L.P. Zhu, Preparation of autoclaved aerated concrete using copper tailings and blast furnace slag, Construction and Building Materials, 2012, **27**(1), 1.
5. T.I. Ugama, S.P. Ejeh and D.Y. Amartey, Effect of iron ore tailing on the properties of concrete, Civil and Environmental Research, 2014, **6**(10), 7.
6. T.I. Ugama and S.P. Ejeh, Iron ore tailing as fine aggregate in mortar used for masonry, International Journal of Advances in Engineering & Technology, 2014, **7**(4), 1170.
7. k.k. Shetty, G. Nayak and V. Vijayan, Effect of red mud and iron ore tailings on the strength of self-compacting concrete, European Scientific Journal, 2014, **10**(21), 168.
8. B.N. Skanda kumar, R. Suhas, S.U. Shet and J.M. Srishailal, Utilization of iron ore tailings as replacement to fine aggregates in cement concrete pavements, International Journal of Research in Engineering and Technology, 2014, **3**(7), 369.
9. C. Li, H.H.Sun, Z.L. Yi and L.T. Li, Innovative methodology for comprehensive utilization of iron ore tailings: Part 2: The residues after iron recovery from iron ore tailings to prepare cementitious material, Journal of Hazardous Materials, 2010, **174**(1-3), 78.
10. Z.L. Yi, H.H.Sun, X.Q. Wei and C. Li, Iron ore tailings used for the preparation of cementitious material by compound thermal activation, International Journal of Minerals, Metallury and Materials, 2009, 16(3), 355.
11. Z.L. Yi, H.H. Sun, C. Li, Y.M. Sun and Y. Li, Relationship between polymerization degree and cementitious activity of iron ore tailings, International Journal of Minerals, Metallury and Materials, 2010, **17**(13), 116.
12. Y.M. Choi, Y.J. Kim, O. Choi, K.M. Lee and M. Lachemi, Utilization of tailings from tungsten mine waste as a substitution material for cement, Construction and Building Materials, 2009, **23**(2), 2481.
13. J.I. Bhatty, J. Marijnissen and K. Reid, Portland cement production using mineral wastes, Cement and Concrete Research, 1985, **15**(3), 501.
14. Z.L. Shi, Z.Y. Luo, X.G. Lin, S.Y. Fu, X.Q. Yuna and K.F. Cen, Experimental study on utilization of metallic tailings as cement mineralizer and iron raw material, Journal of Zhejiang University(Engineering Science), 2010, **42**(3), 506.
15. Y.L. Chen, Y.M. Zhang, T.J. Chen, Y.L. Zhao and S.X. Bao, Preparation of eco-friendly construction bricks from hematite tailings, Construction and Building Materials, 2011, **25**(4), 2107.
16. Y.L. Zhao, Y.M. Zhang, T.J. Chen and S.X. Bao, Preparation of high strength autoclaved bricks from hematite tailings, Construction and Building Materials, 2012, **28**(1), 450.
17. B.G. Ma and Z. Xu, Study on a new kind of aerated concrete containing efflorescence sand-phosphorus slag-lime, Journal of Building Matererials, 1999, **2**(3), 223.
18. N.Y. Mostafa, Influence of air-cooled slag on physicochemical properties of autoclaved aerated concrete, Cement Concrete Research, 2005, **35**(7),1349.
19. F.X. Li, Y.Z. Chen and S.Z. Long, Experimental investigation on aerated concrete with addition of lead–zinc tailings, Journal of Southwest Jiaotong University, 2008, **43**(6), 810.
20. General Administration of Quality Supervision, Inspection and Quarantineof the People's Republic of China, Standardization Administration of the People's Republic of China, GB/T 11968-2008 Autoclaved aerated concrete blocks, China Planning Press, Beijing, 2006.
21. J. Bensted, P. Barnes, Structure and Performance of Cements, second ed., Spon Press, New York, 2002.
22. Wang C L, Ni W, Zhang S Q, Wang S, Gai G S, Wang W K. Preparation and properties of autoclaved aerated concrete using coal gangue and iron ore tailings, J. Construction and Building Materials, 2016, **104,** 109.
23. P.Y. Yan, J. Peng and X. Qin, Preconditions of the harmful effect induced by delayed ettringite formation in massive shrinkage-compensating concrete, Journal of the Chinese Ceramic Society. 2001, **29**(2), 109.
24. R. Siauciunas and A. Baltusnikas, Influence of SiO_2 modification on hydrogarnets formation during hydrothermal synthesis, Cement Concrete Research, 2003, **33**(11), 1789.
25. N. Meller, K. Kyritsis and Hall C, The mineralogy of the $CaO-Al_2O_3-SiO_2-H_2O$ (CASH) hydroceramie system from 200 to 350 ℃, Cement Concrete Research, 2009, **39**(1), 45.
26. Z.J. Zhang, C.J. Ke, P.A. Liu and M.F. Zhong, Analysis and mechanism of hydrogarnets formation and transformation in autoclaved reaction, Journal of Instrumental Analysis, 2008, **28**(9), 1008.
27. D.Z. Li, W. Ni, J.W. Zhang, H. Wu and Y.Y. Zhang, The phase transformation of iron ore tailings during autoclaved curing, Journal of the Chinese Ceramic Society, 2011, **39**(4), 708.
28. M. Singh and M. Grag, Acitvaiton of gypsum anhydrite-slag mixtures, Cement and Concrete Research, 1995, **25**(2), 332.
29. M.D. Li and Y. Qin, The identifieation of phase transition types by differential thermal analysis, Materials Review, 1996, (4), 79.
30. D.S. Klimesch and A. Ray, DTA-TGA evaluations of the $CaO-Al_2O_3-SiO_2-H_2O$ system treated hydrothermally, Thermochim Acta, 1999, **334** (1-2), 115.
31. X.M. Liu, H.H. Sun, X.P. Feng and N. Zhang, Relationship between the microstructure and reaction performance of aluminosilicate, International Journal of Minerals, Metallurgy and Materials, 2010, **17**(1), 108.

****